Peptidylarginine deiminase 2-catalyzed histone H3 arginine 26 citrullination facilitates estrogen receptor α target gene activation

Xuesen Zhang[a], Michael Bolt[b], Michael J. Guertin[c], Wei Chen[d], Sheng Zhang[d], Brian D. Cherrington[a,1], Daniel J. Slade[e], Christina J. Dreyton[e], Venkataraman Subramanian[e], Kevin L. Bicker[e], Paul R. Thompson[e], Michael A. Mancini[b], John T. Lis[c], and Scott A. Coonrod[a,2]

[a]Baker Institute for Animal Health, College of Veterinary Medicine, [c]Department of Molecular Biology and Genetics, and [d]Proteomics and Mass Spectrometry Core Facility, Cornell University, Ithaca, NY 14853; [b]Department of Molecular and Cellular Biology, Baylor College of Medicine, Houston, TX 77030; and [e]Department of Chemistry, The Scripps Research Institute, Jupiter, FL 33458

Edited by Jerry L. Workman, Stowers Institute for Medical Research, Kansas City, MO, and accepted by the Editorial Board July 2, 2012 (received for review February 24, 2012)

Cofactors for estrogen receptor α (ERα) can modulate gene activity by posttranslationally modifying histone tails at target promoters. Here, we found that stimulation of ERα-positive cells with 17β-estradiol (E2) promotes global citrullination of histone H3 arginine 26 (H3R26) on chromatin. Additionally, we found that the H3 citrulline 26 (H3Cit26) modification colocalizes with ERα at decondensed chromatin loci surrounding the estrogen-response elements of target promoters. Surprisingly, we also found that citrullination of H3R26 is catalyzed by peptidylarginine deiminase (PAD) 2 and not by PAD4 (which citrullinates H4R3). Further, we showed that PAD2 interacts with ERα after E2 stimulation and that inhibition of either PAD2 or ERα strongly suppresses E2-induced H3R26 citrullination and ERα recruitment at target gene promoters. Collectively, our data suggest that E2 stimulation induces the recruitment of PAD2 to target promoters by ERα, whereby PAD2 then citrullinates H3R26, which leads to local chromatin decondensation and transcriptional activation.

Cancers of the female reproductive system are serious human health problems, and estrogen plays a critical role in the initiation and progression of these diseases (1). Despite decades of research into mechanisms of 17β-estradiol (E2)-responsive gene transcription, our understanding of this process is far from complete (2). It is generally believed that, upon E2 binding, the nuclear hormone receptor estrogen receptor α (hereafter called ER) undergoes major structural reorganization, associates with estrogen-response elements (ERE) within target gene promoters, and recruits a range of coactivators including histone modification enzymes (3–6). After deposition, the resulting histone modifications can then modulate target gene activity by affecting local chromatin structure and regulating the accessibility of chromatin to transcription factors (2, 5, 7–9).

Peptidylarginine deiminase (PAD) enzymes convert arginine and methylarginine residues to citrulline via a hydrolytic process termed citrullination or deimination (10, 11). We and others have shown that one such PAD, PAD4, appears to play a repressive role in regulating the expression of the canonical ER target gene, TFF1, via citrullination of histone H4 methylarginine 3, thus suggesting that PADs potentially function as ER cofactors (12, 13). Given that these previous studies were limited to a single ER target promoter, we chose to take a more comprehesive approach to test whether PAD-mediated histone tail citrullination may be more fundamental to ER target gene regulation than previously realized. In this study, we show that citrullination of histone H3R26 at ER targets is closely associated with gene transcription and that citrullination at this residue is catalyzed by PAD2, as opposed to PAD4. Additionally, we show that PAD2 interacts with ER and that PAD2-mediated citrullination of H3R26 likely facilitates transcriptional activation by creating an open, permissive, chromatin architecture around the EREs of E2-induced genes.

Results and Discussion

Estrogen Induces H3R26 Citrullination in Cellulo and in Vivo. To begin testing for associations between histone citrullination and E2 signaling, we first investigated whether estrogen stimulation globally induced citrullination of specific histone arginine residues in MCF-7 breast cancer cells by using confocal immunofluorescence with three different site-specific anticitrullinated histone antibodies: anti-H3Cit2/8/17, anti-H3Cit26, and anti-H4Cit3. Results showed that 45 min of E2 treatment induced a pronounced increase of H3Cit26 in the nuclei of cells (Fig. S1), whereas staining with the two other anticitrullinated histone antibodies was not visibly affected (Fig. S2 *A* and *B*). Interestingly, after E2 stimulation, we also did not observe global differences in three other histone modifications known to be altered at specific promoters by E2: H4K5acteyl, H3K9dimethyl, and H3K27trimethyl (Fig. S2 *C*–*E*). Further, the increase in H3Cit26 levels was observed as early as 5 min after E2 stimulation and appeared to peak at 45 min (Fig. S3). This time frame is consistent with recent reports on the dynamics of estrogen signaling whereby changes in the MCF-7 cell transcriptome were observed by GRO-seq analysis within 10 min of E2 stimulation (14).

Given these exciting results, and the relatively uncharacterized nature of the anti-H3Cit26 antibody, we next further validated the specificity of this antibody by treating MCF-7 cell histones with recombinant human PAD2 and then immunoblotting the resolved proteins with the H3Cit26 antibody (Note: Our rationale for using PAD2 as opposed to PAD4 is described below). Results (Fig. S4*A*) show that this antibody was reactive with an appropriately sized band from the PAD2-citrullinated histones but was not reactive with untreated histones. Further, we also found that preincubation of the anti-H3Cit26 antibody with the cognate citrullinated peptide nearly completely blocked detection of the H3Cit26 modification. The protein band corresponding to the mass of the citrullinated histone was then excised from the gel and evaluated by mass spectroscopic (MS) analysis. Results show that citrulline was readily detected on histone H3 peptides (24-AAR

Author contributions: X.Z. and S.A.C. designed research; X.Z., M.B., B.D.C., D.J.S., C.J.D., V.S., K.L.B., and P.R.T. performed research; X.Z., M.J.G., W.C., S.Z., M.A.M., and J.T.L. analyzed data; and X.Z., M.J.G., J.T.L., and S.A.C. wrote the paper.

The authors declare no conflict of interest.

This article is a PNAS Direct Submission. J.L.W. is a guest editor invited by the Editorial Board.

Data deposition: The data reported in this paper have been deposited in the Gene Expression Omnibus (GEO) database, www.ncbi.nlm.nih.gov/geo (accession no. GSE32599).

[1]Present address: Department of Zoology and Physiology, University of Wyoming, Laramie, WY 82071.

[2]To whom correspondence should be addressed. E-mail: sac269@cornell.edu.

This article contains supporting information online at www.pnas.org/lookup/suppl/doi:10.1073/pnas.1203280109/-/DCSupplemental.

[Cit]K[acetyl]SAPATGGVK-36) from the PAD2-treated sample (Fig. S4*B*). We note here that the H3Cit26 modification only occurred on H3 peptides that contained an acetyl modification at lysine-27, thus raising the possibility that a functional "cross talk" exists between the H3Cit26 and H3K27acetyl modifications. To confirm that the anti-H3Cit26 antibody was not recognizing other citrullinated residues on chromatin, we also preblocked the anti-H3Cit26 antibody by using unmodified H3 (19–38), H3Cit26, or H3Cit2/8/17 peptides and then performed chromatin immunoprecipitation (ChIP) analysis on the TFF1 ERE promoter region. Results (Fig. S4*C*) showed that only the H3Cit26 peptide abolished the detection of H3Cit26 at the TFF1 ERE. Taken together, these results strongly suggest that the H3Cit26 antibody is specifically reactive with the H3Cit26 modification.

To investigate whether our findings may have physiological relevance in vivo, we next treated ovariectomized mice with exogenous E2 pellets and then carried out immunohistochemical analysis of uterine tissue (a major E2 target) by using the anti-H3Cit26 antibody. As predicted, relative to vehicle-treated animals, we observed a strong increase in H3Cit26 staining in the nucleus of uterine epithelial cells after E2 treatment (Fig. 1*A*). Therefore, both our in vitro and in vivo observations strongly suggest that citrullination of histone H3R26 is specifically and globally induced by estrogen signaling.

Estrogen-Induced H3R26 Citrullination Is Associated with ER Activity. Given that the effects of E2 on gene regulation are primarily mediated by ER, we next investigated the relationship between H3Cit26 and ER in cells. After E2 stimulation, immunofluorescence analysis showed a strong colocalization between H3Cit26 and ER in MCF-7 cells (Fig. 1*B*). In ER-negative MDA-MB231 breast cancer cells, however, citrullination of H3R26 was not observed, either before or after E2 stimulation (Fig. 1*C*). We further confirmed the requirement of ER for H3R26 citrullination by using HeLa cells, which are also ER negative (Fig. 1*D*). As expected, H3R26 citrullination was not observed in these cells either before or after E2 treatment. However, in HeLa cells that stably overexpress recombinant ER, E2 stimulation resulted in a robust citrullination of H3R26 (Fig. 1*E*). Thus, our data strongly suggest citrullination of H3R26 depends on E2-ER signaling.

We next investigated the dynamics of estrogen-ER–mediated H3R26 citrullination by using another HeLa cell line that contains multiple genomically integrated copies of the estrogen-responsive prolactin (PRL) enhancer/promoter reporter array (Fig. 1*F*) and a stably expressed ER-GFP-fusion construct (GFP-ER) (15). This line allows for the imaging of GFP-ER binding to the PRL array and subsequent large-scale changes in chromatin structure. Results from previous studies found that E2 stimulation induces an ER-dependent decondensation of the PRL array, thus reflecting a chromatin state similar to that found at endogenous ER target promoters during transactivation. Interestingly, previous studies demonstrated that levels of specific histone acetylation and methylation marks are not greatly altered at the PRL array after E2 stimulation (16). In our study, before E2 stimulation, little citrullination of H3R26 was observed. However, after E2 treatment, a large H3Cit26 foci was found to strongly colocalize with GFP-ER at the decondensed PRL array (Fig. 1*F* and Fig. S5). Given our recent finding that PAD-dependent histone hypercitrullination results in chromatin decondensation (17), we predicted that the targeting of ER to the PRL array by estrogen likely resulted in ER-mediated recruitment of PADs to the promoter and subsequent PAD-mediated citrullination of H3R26, thus resulting in decondensation of the PRL array.

ERE Motifs Overlap H3Cit26 Sites at E2-Induced Gene Promoters. Given the observed global associations between histone citrullination and estrogen signaling, we next began to investigate the extent to which H3R26 citrullination correlates with ER binding at proximal promoter target regions by conducting ChIP/promoter analysis in MCF-7 cells using a tiling array that covers 2.2 kb upstream and 500 bp downstream, relative to the transcription start sites (TSS) (18). Comparison of citrullination at H3R26

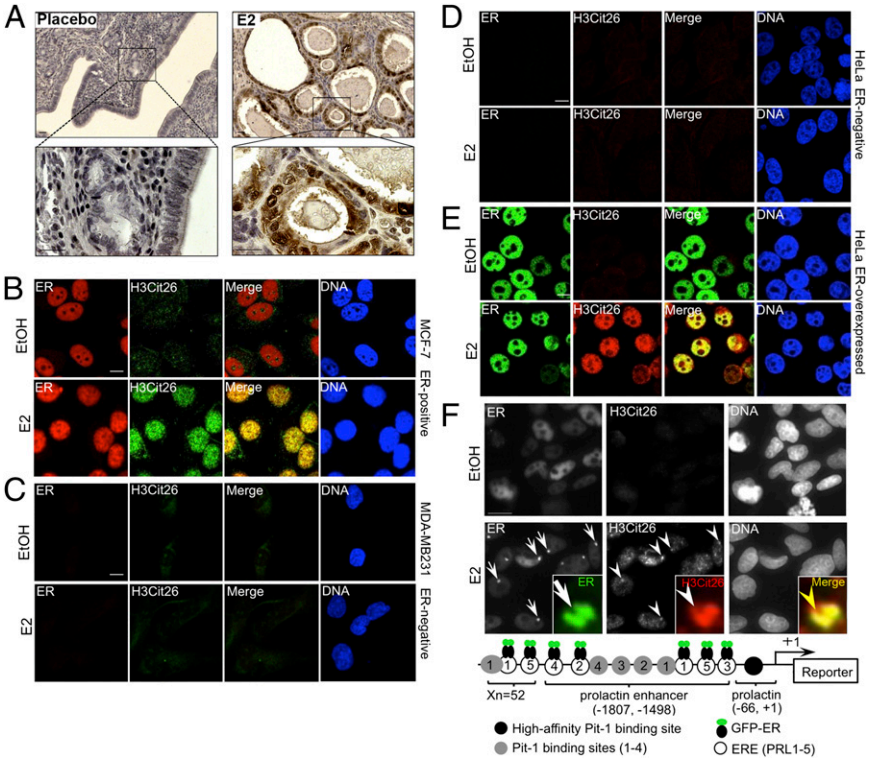

Fig. 1. Estrogen-induced H3R26 citrullination is associated with ER. (*A*) IHC analysis of H3Cit26 staining on uterine sections collected from ovariectomized mice implanted with pellets containing either vehicle control or E2 pellets. (Scale bars: 20 μm.) (*B–E*) Confocal microscopic analyses showing colocalization of H3Cit26 and ER in nuclei of ER-positive MCF-7 cells (*B*). This colocalization is not observed in either ER-negative MDA-MB231 (*C*) or HeLa (*D*) cells upon E2 stimulation. Stable overexpression of ER in HeLa cells (*E*) restores E2-induced citrullination of H3R26. Merged images highlight H3Cit26 and ER colocalization. (Scale bar: 10 μm.) (*F*) Colocalization of H3Cit26 and GFP-ER at a decondensed PRL-array in HeLa cells stably overexpressing GFP-ER. Arrows indicate GFP-ER, and arrowheads indicate H3Cit26 foci in the decondensed array after E2 stimulation. (Scale bar: 15 μm.) *Inset* highlights a single PRL-array locus. (Magnification: 10×.) Yellow arrowhead represents the coincident anti-H3Cit26 (red) and GFP-ER (green) staining. Schema in *Lower* shows the essential elements of the PRL-based array (16). Xn indicates 52 repeats of the elements.

before and after E2 stimulation revealed 208 promoters that contained significantly higher levels of the H3Cit26 modification after E2 treatment (induced), 110 promoters with lower H3Cit26 levels after E2 treatment (reduced), and 55 promoters with no changes in H3Cit26 levels (constitutive) (Fig. 2 *A* and *B*). To further characterize the putative targets of H3Cit26-regulated gene transcription, we used de novo motif discovery to search for overrepresented motifs within 100 bp of the center of the H3Cit26 peaks (19). This unbiased analysis revealed the presence of a previously published, well-characterized ERE motif (20) (Fig. 2*C*). The heatmap in Fig. 2*D* demonstrates that the ERE motif displayed a similar distribution pattern as that of H3Cit26 in the induced group (top left to lower right diagonal), and this pattern was not observed in the noninduced groups (reduced and constitutive). We identified 59 targets (28.4%) as having an ERE in the H3Cit26-induced group, whereas only 8 (4.8%) genes in the noninduced groups contained the ERE motif, thus indicating a 5.9-fold ERE enrichment in the H3Cit26-induced group (Fisher's exact test, $P = 7.5 \times 10^{-10}$) (Fig. 2*E*). Collectively, these data support the hypothesis that E2-induced citrullination at H3R26 plays a role modulating the expression of a subset of ER target genes. Given that ER can bind to chromatin through bridging interactions with other transcription factors, such as AP-1, for example, and that these ER binding sites often do not contain underlying EREs (21), it seems likely that the H3Cit26 modification is also enriched at other non-ERE–containing target sites. Additionally, a recent ChIP-seq report found that only ~7% of ER binding sites are within 5 kb upstream of the TSS (22). Given that the proximal promoter arrays used in our study only covered 2.2 kb upstream of the TSS, it seems likely that many ER target sites outside of this region are also citrullinated at H3R26 after E2 treatment.

H3R26 Citrullination Likely Promotes an Open Chromatin Architecture at the EREs of E2-Induced Gene Promoters. A growing body of evidence suggests that specific histone tail modifications function, in part, by "loosening" the chromatin architecture at gene promoters, thus enhancing accessibility for binding factors, such as basal and specific transcription factors and RNA polymerases (2, 5, 7–9). Micrococcal nuclease (MNase) cleaves linker and nucleosome-free DNA, and is, therefore, often used to evaluate the state of chromatin compaction (23, 24). To test the hypothesis that H3R26 citrullination might act to maintain an open chromatin architecture around ERE regions at the promoters of a subset of E2-induced genes, we next examined the accessibility of ERE-containing H3Cit26-bound promoters to digestion by MNase as described (23, 24). We tracked five ER targets from the induced group that contain well-characterized EREs in their promoters, TFF1 (25), KRT13 (26), GREB1 (27), WISP2 (28), and CYP1B1 (29, 30) and also two control genes, SCN1A *and* VAT1L, which did not show an increase or decrease in citrullination after E2 treatment and do not appear to contain an ERE near the citrullinated site (i.e., the noninduced group). As expected, E2 treatment caused a significant decrease in MNase

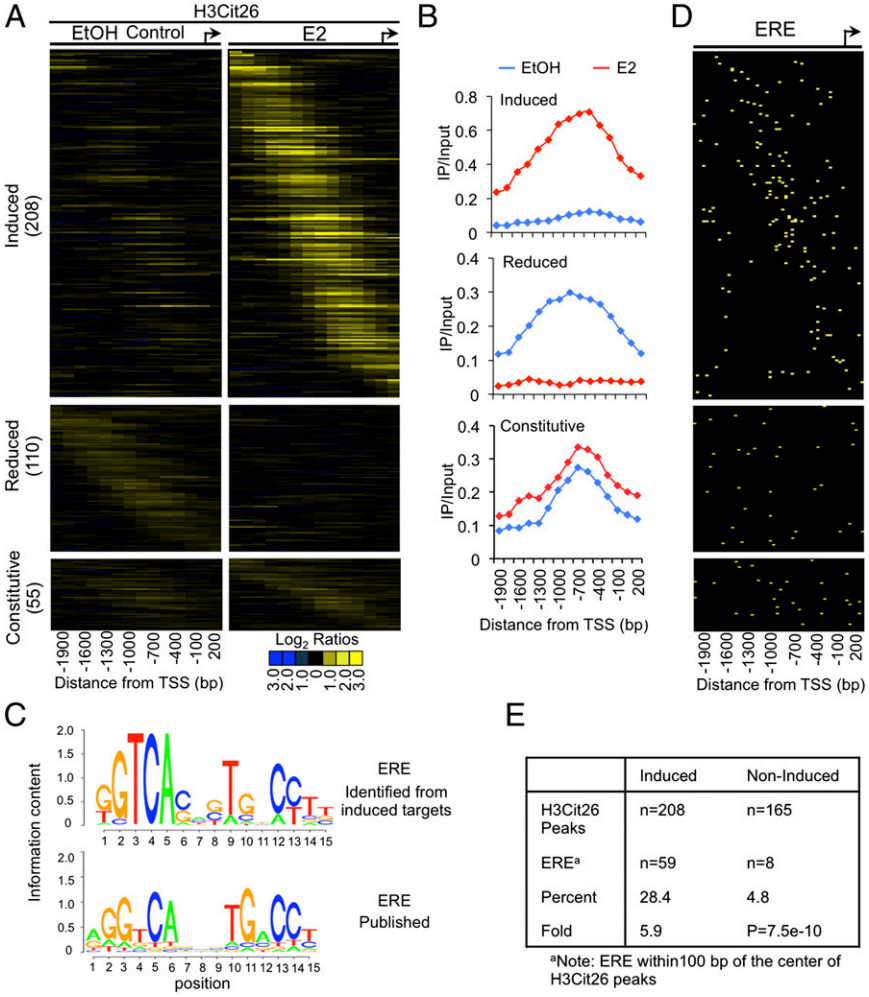

	Induced	Non-Induced
H3Cit26 Peaks	n=208	n=165
ERE[a]	n=59	n=8
Percent	28.4	4.8
Fold	5.9	P=7.5e-10

[a]Note: ERE within100 bp of the center of H3Cit26 peaks

Fig. 2. Genome-wide location analysis of transcriptional targets for H3R26 citrullination in MCF-7 cells reveals ERE motifs overlapping the H3Cit26 sites at E2-induced gene promtoers. (*A*) Heat maps of anti-H3Cit26 ChIP-chip data showing the significant H3Cit26 peaks across target promoters from −2200 to +500 bp relative to the TSS before (EtOH Control) and after E2 treatment. The genes in each group (*y* axis) are ordered from those with the 5′-most H3Cit26 peak to those with the 3′-most peak. (*B*) Averaging of peak centered ChIP-chip data across the groups in *A* illustrates the distinct patterns of H3R26 citrullination at target promoters in response to E2. (*C*) De novo determination of DNA sequence motif associated with H3Cit26 at the E2-induced targets reveals a consensus ERE motif. *C Lower* shows a published ERE motif (20). (*D*) Heat maps of significant EREs that overlap with the H3Cit26 peak. EREs are ordered according to H3Cit26 heat maps. (*E*) Percentage and fold enrichment of EREs in the E2-induced and noninduced H3Cit26 datasets.

protection at the ERE region on the promoters of the E2-induced genes relative to the EtOH control (Fig. 3 *A* and *B* and Fig. S6 *A*–*C*), and this effect was not observed at the noninduced control promoters (Fig. 3 *A* and *B* and Fig. S6*D*). This observation suggests that, after E2 treatment, H3R26 citrullination at the ERE regions of E2-induced gene promoters results in a MNase hypersensitivity profile that is indicative of an open chromatin architecture. Moreover, ChIP analysis (Fig. 3 *C* and *D*) revealed that, after E2 stimulation, there were marked increases in ER binding and H3R26 citrullination at the ERE regions on TFF1 and KRT13 promoters. Although E2 weakly induced the recruitment of ER to *SCN1A,* increased citrullination at H3R26 was not observed, thus further confirming our promoter array analysis. Taken together, our data suggest that E2-induced citrullination of H3R26 helps to establish an open and active chromatin environment at ER target promoters.

Interdependent PAD2-Catalyzed H3R26 Citrullination and ER Recruitment at Induced Target Promoter EREs Facilitates Target Gene Transcription. We next pretreated MCF-7 cells with the pure ER antagonist, ICI182780, and then performed ChIP to test for potential E2-induced functional interplay between ER and H3R26 citrullination at EREs. As shown in Fig. 4 *A* and *B*, although E2 is able to induce both H3R26 citrullination and ER recruitment at TFF1 and KRT13, inhibiting ER blocked not only ER recruitment, but also strongly suppressed H3R26 citrullination at this region. H3R26 citrullination at the SCN1A promoter was not affected by any treatment. These data indicate that E2-induced recruitment of ER to a subset of responsive gene promoter EREs facilitates H3R26 citrullination at these sites.

We then wondered whether decreased H3R26 citrullination could have a similar inhibitory effect on ER recruitment. To address this question, however, we first needed to identify which PAD was responsible for catalyzing H3R26 citrullination. Although most previous reports have documented a role for PAD4 in gene regulation via histone citrullination (12, 13), we have recently found that PAD2 also appears to citrullinate histones in vivo (31). This finding raised the possibility that the observed citrullination at H3R26 might be mediated by PAD2 as opposed to PAD4. To test this hypothesis, we first evaluated the substrate preferences of these enzymes by determining the steady-state kinetic parameters for histones H3 and H4, as well as several peptides whose sequences are based on the N-termini of these proteins and encompass residues known to be citrullinated (Table S1).

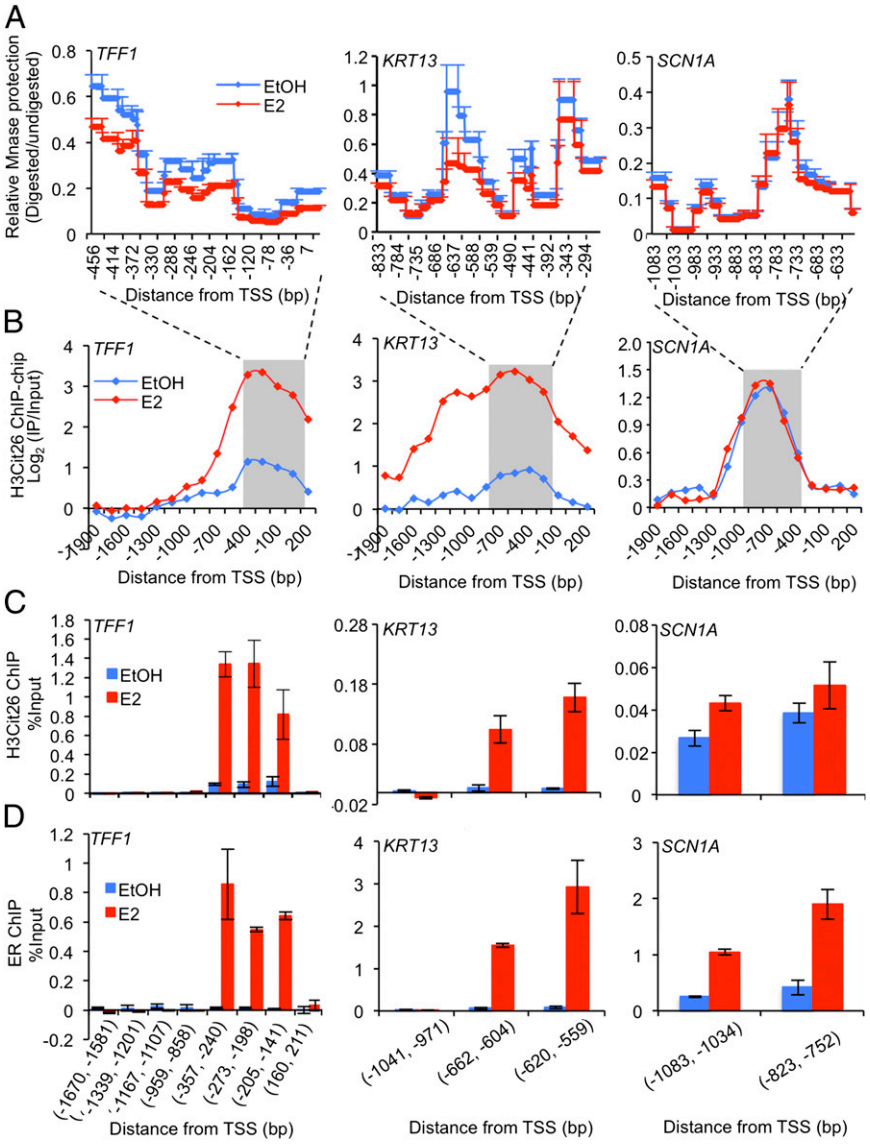

Fig. 3. After estrogen stimulation, H3R26 citrullinaton facilitates an open chromatin architecture at the EREs of E2-induced gene promoters. (*A*) MNase protection assay after EtOH and E2 treatment in MCF-7 cells. qPCR was performed to tile through the proximal promoter ERE region with overlapping amplicons (~100-bp PCR product average, with ~20 bp overlap). Relative ratio of the amount of digested DNA to genomic control was used to determine the extent of MNase protection. Values from overlapping primer sets are averaged. Each point represents the mean + SEM, $n = 3$. (*B*) H3Cit26 ChIP-chip signals localize to the proximal promoter ERE regions of E2-induced targets. The shaded region indicates the range tested in *A* for MNase protection assay. (*C* and *D*) ChIP-qPCR analysis of H3Cit26 and ER at target gene promoters after EtOH or E2 treatment in MCF-7 cells. Error bars indicate SEM, $n = 3$.

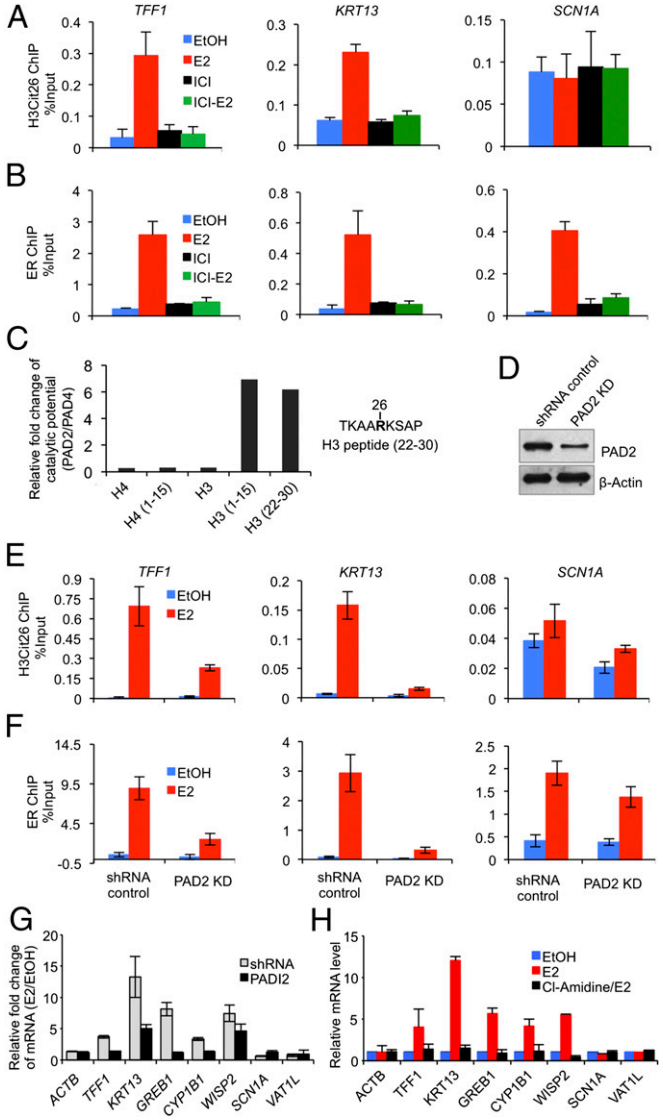

Fig. 4. Interdependent H3R26 citrullination catalyzed by PAD2 and ER targeting at induced target promoter EREs facilitates target gene transcription after stimulation of MCF-7 cells with E2. (*A* and *B*) ChIP-qPCR analysis of H3Cit26 and ER at target gene promoters showing that complete inhibition of ER by ICI182780 (ICI) also inhibits H3R26 citrullination at EREs. (*C*) Plots of the ratio of the catalytic efficiencies ($k_{cat}/K_{m(PAD2)}$ / $k_{cat}/K_{m(PAD4)}$) showing the substrate specificity of PAD2 and PAD4. (*D*) Western blot showing shRNA-mediated depletion of PAD2 in MCF-7 cells. (*E* and *F*) ChIP-qPCR analysis of H3Cit26 and ER at target gene promoters showing that depletion of PAD2 not only decreases H3Cit26 but also suppresses ER recruitment to EREs at target gene promoters. (*G* and *H*) Relative mRNA expression (RT-qPCR) analyses in EtOH or E2-stimulated MCF-7 cells with or without PAD2 knockdown (*G*); with or without Cl-Amidine treatment (*H*). Expression data were normalized to GAPDH transcripts, and the graph represents the relative fold enrichment over vehicle treated. Error bars indicate SEM, $n = 3$.

Analysis of the ratio of catalytic efficiencies ($k_{cat}/K_{m(PAD2)}$ / $k_{cat}/K_{m(PAD4)}$) reveals that PAD2 citrullinates the H3 (22–30) peptide, which contains H3R26, at a sixfold higher rate than PAD4 (Fig. 4*C*), indicating that the histone H3R26 residue is a valid PAD2 target in vitro. To test whether PAD2 might target H3R26 *in cellulo*, we then generated PAD2- (Fig. 4*D*) and PAD4- (18) depleted MCF-7 cell lines and performed ChIP analysis on the TFF1 and KRT13 promoters. Results from the PAD2-depleted line showed a marked suppression of H3R26 citrullination at TFF1 and KRT13 after E2 stimulation (Fig. 4*E*). Similar effects, however, were not observed in the PAD4 depleted line (Fig. S7). Taken together, our in vitro and *in cellulo* findings support our hypothesis that PAD2 (as opposed to PAD4) plays a direct role in citrullinating H3R26 in cells. Importantly, we also found that PAD2 depletion markedly suppressed ER recruitment to EREs at the TFF1 and KRT13 promoters (Fig. 4*F*). This result indicates that PAD2-mediated citrullination of H3R26 is likely to be involved in recruitment of ER to the ERE.

One interpretation of our cumulative findings is that PAD2-mediated H3R26 citrullination opens the local chromatin architecture, thus facilitating ER recruitment. Alternatively, however, it is also possible that ER recruitment may induce a chromatin remodeling event that, in turn, yields a chromatin template that is accessible to citrullination at H3R26. In light of the recent "assisted loading" hypothesis (32), it is possible that both models are functional and this dual activity produces a reinforcing loop that ultimately enhances ER binding that, in turn, recruits the requisite coactivator complexes that create the appropriate chromatin environment for binding by the general transcriptional machinery and RNA polymerase. The interdependent nature of E2-stimulated H3R26 citrullination and ER recruitment at induced gene promoters also suggests a potential association between PAD2 and ER. To test this hypothesis, we first performed coimmunoprecipitation analysis in MCF-7 cells and found that endogenous PAD2 does appear to interact with endogenous ER and that this interaction is enhanced after E2 treatment (Fig. S8*A*). Reciprocally, we also generated an MCF-7 cell line that stably overexpresses a Flag-tagged version of PAD2 and found that E2 stimulates the interaction between endogenous ER and Flag-PAD2 (Fig. S8 *B* and *C*). We note here that the Flag-tagged PAD2 approach was necessary because immunoprecipitation-quality PAD2 antibodies are not available. We then carried out ChIP analysis by using the anti-Flag antibody in this modified MCF-7 cell line and found that, after E2 stimulation, Flag-tagged PAD2 was specifically recruited to the same sites within the ERE region of TFF1 that are bound by ER and contain the H3Cit26 modification (Fig. S8*D*). The observations that E2-induced chromatin decondensation is closely related to transcriptional activity (33) and that the H3Cit26 modification was primarily observed at the ERE regions of E2-induced genes suggested that PAD2-mediated citrullination of H3R26 at ERE promoter regions facilities ER-mediated gene transactivation. To test this hypothesis, we investigated whether the transcription of genes, whose promoters were citrullinated after E2 treatment, was affected by either PAD2 depletion or inhibition. As expected, either knockdown of PAD2 (Fig. 4*G*) or pretreatment of cells with Cl-Amidine, a newly developed arginine-based PAD inhibitor (34) (Fig. 4*H*), dramatically dampened the ability of these ER targets to be activated after E2 treatment.

Taken together, our data indicate that PAD2 plays an important role in mediating the activation of ER target genes via citrullination of histone H3R26. This activity likely cooperates with other activities such as cofactor binding, chromatin remodeling factor association, and basal transcription factor/RNA polymerase recruitment in establishing an open, permissive, chromatin architecture around the EREs of E2-induced genes, thus facilitating transcriptional activation. These findings help to improve our mechanistic understanding of how ER regulates gene transcription via altering chromatin structure.

Materials and Methods

Cell Culture. Cell culture, shRNA, and Flag-tagged PAD2 overexpression are described in *SI Materials and Methods*. Before E2 treatment, cells were cultured for 3 d in DMEM phenol red-free medium supplemented with 10% (vol/vol) charcoal-dextran-treated calf serum. ICI182780 was used at 10 μM for 18 h before the addition of E2. Cl-Amidine was used at 200 μM for 40 h before E2 stimulation.

Mouse Ovariectomy, E2 Treatment, and Immunohistochemistry (IHC). All procedures were conducted in accordance with the National Institutes of Health regulations and approved by the Cornell University animal use committee. See *SI Materials and Methods* for detailed protocols.

Confocal Microscopy. Cells grown on slides were subjected to E2 treatment for 45 min. Confocal microscopy experiments were described (13). Antibodies used are listed in *SI Materials and Methods*.

High Content Analysis-Based Immunofluorescence Microscopy. Stable GFP-ERα: PRL-HeLa cells were E2 starved and then treated for 30 min with either 10 nM E2 or ethanol. Immunofluorescence experiment, fluorescent microscopy image acquisition, and quantitation was performed as described (15). Nuclear masks were created by using the DAPI channel, and GFP-ER signal was used to define the for PRL array mask. Average intensity measurements were taken (>1,000 cells per treatment) for the nucleoplasmic and array H3Cit26 signals (in E2) and normalized to EtOH nucleoplasm H3Cit26 signal.

ChIP and ChIP-chip. ChIP experiments were performed as described (18). E2 was used at concentration of 100 nM for 45 min; antibodies and quantitative PCR (qPCR) primers are listed in *SI Materials and Methods*. ChIP for H3Cit26 coupled with hybridization to a human HG18 RefSeq promoter microarray from Nimblegen and genomic data analyses were performed as described (18). Significant peaks and the "induced," "reduced," or "constitutive" regions were defined as described in *SI Materials and Methods*. The TSS-anchored ChIP-chip heat maps were generated by using 600-bp windows with 150-bp steps and were visualized with Java Treeview (35). The data can be accessed through the NCBI/GEO website by using accession no. GSE32599.

De Novo Motif Search. MEME was applied with all default parameters to search for overrepresented motifs (19). A motif width between 6 and 20 bp was specified by using 200-bp windows centered on each of the 208 induced H3Cit26 binding sites. Table S2 includes the matrix that was found by MEME and subsequently used to make the sequence logo for ERE (Fig. 2*C*) using the R package "seqLogo" contributed by Oliver Bembom (University of California, Berkeley, CA). For the heat map to visualize the ERE distribution, we used a published position-specific weight matrix (20) and searched for the matched that conform with a P value ≤ 0.00005. The promoters were separated into nonoverlapping 50-bp windows and, if an ERE motif was found within a window, the window was colored yellow.

MNase Protection Assay. Estrogen-starved MCF-7 cells were treated with ethanol or 100 nM E2 for 45 min, and MNase protection assay was performed as described (23, 24). MNase was from New England Biolabs (M0247). See primers in *SI Materials and Methods*.

Gene-Specific Expression Analyses. Estrogen-starved cells were treated with ethanol or 100 nM E2 for 6 h. RNA reverse transcription and quantitative real-time PCR were performed as described (18). Primers used are listed in *SI Materials and Methods*.

Steady-State Kinetic Assays. Histone peptides were synthesized by using the Fmoc approach and purified by reverse-phase HPLC. PADs 2 and 4 purification, kinetic assays were performed as described in *SI Materials and Methods*.

Histone Extraction, PAD Assay, Mass Spectrometry, and Immunoprecipitation Assay. See *SI Materials and Methods* for detailed protocols.

ACKNOWLEDGMENTS. We thank W. L. Kraus for HeLa-ER cells and C. D. Allis for the H3 unmodiffied peptide. This work was supported by a Department of Defense Era of Hope Scholar Award W871XWH-07-1-0372 (to S.A.C.), and National Institutes of Health Grants GM25232 (to J.T.L.) and GM079357 (to P.R.T.). X.Z. was supported by a Postdoctoral Fellowship KG101303 from Susan G. Komen for the Cure, and M.B. was supported by Training Fellowship T15LM007093 from the Keck Center National Library of Medicine Training Program in Biomedical Informatics of the Gulf Coast Consortia.

1. Cooke PS, Buchanan DL, Lubahn DB, Cunha GR (1998) Mechanism of estrogen action: Lessons from the estrogen receptor-alpha knockout mouse. *Biol Reprod* 59:470–475.
2. Green KA, Carroll JS (2007) Oestrogen-receptor-mediated transcription and the influence of co-factors and chromatin state. *Nat Rev Cancer* 7:713–722.
3. Brzozowski AM, et al. (1997) Molecular basis of agonism and antagonism in the oestrogen receptor. *Nature* 389:753–758.
4. Mann M, Cortez V, Vadlamudi RK (2011) Epigenetics of estrogen receptor signaling: Role in hormonal cancer progression and therapy. *Cancers (Basel)* 3:1691–1707.
5. Métivier R, et al. (2003) Estrogen receptor-alpha directs ordered, cyclical, and combinatorial recruitment of cofactors on a natural target promoter. *Cell* 115:751–763.
6. Wiench M, Miranda TB, Hager GL (2011) Control of nuclear receptor function by local chromatin structure. *FEBS J* 278:2211–2230.
7. Guertin MJ, Lis JT (2010) Chromatin landscape dictates HSF binding to target DNA elements. *PLoS Genet* 6:e1001114.
8. Li B, Carey M, Workman JL (2007) The role of chromatin during transcription. *Cell* 128: 707–719.
9. Strahl BD, Allis CD (2000) The language of covalent histone modifications. *Nature* 403: 41–45.
10. Klose RJ, Zhang Y (2007) Regulation of histone methylation by demethylimination and demethylation. *Nat Rev Mol Cell Biol* 8:307–318.
11. Zhang Y (2004) Molecular biology: No exception to reversibility. *Nature* 431:637–639.
12. Cuthbert GL, et al. (2004) Histone deimination antagonizes arginine methylation. *Cell* 118:545–553.
13. Wang Y, et al. (2004) Human PAD4 regulates histone arginine methylation levels via demethylimination. *Science* 306:279–283.
14. Hah N, et al. (2011) A rapid, extensive, and transient transcriptional response to estrogen signaling in breast cancer cells. *Cell* 145:622–634.
15. Ashcroft FJ, Newberg JY, Jones ED, Mikic I, Mancini MA (2011) High content imaging-based assay to classify estrogen receptor-α ligands based on defined mechanistic outcomes. *Gene* 477:42–52.
16. Sharp ZD, et al. (2006) Estrogen-receptor-alpha exchange and chromatin dynamics are ligand- and domain-dependent. *J Cell Sci* 119:4101–4116.
17. Wang Y, et al. (2009) Histone hypercitrullination mediates chromatin decondensation and neutrophil extracellular trap formation. *J Cell Biol* 184:205–213.
18. Zhang X, et al. (2011) Genome-wide analysis reveals PADI4 cooperates with Elk-1 to activate c-Fos expression in breast cancer cells. *PLoS Genet* 7:e1002112.
19. Bailey TL, et al. (2009) MEME SUITE: Tools for motif discovery and searching. *Nucleic Acids Res* 37(Web Server issue):W202-8.
20. Grober OM, et al. (2011) Global analysis of estrogen receptor beta binding to breast cancer cell genome reveals an extensive interplay with estrogen receptor alpha for target gene regulation. *BMC Genomics* 12:36.
21. Paech K, et al. (1997) Differential ligand activation of estrogen receptors ERalpha and ERbeta at AP1 sites. *Science* 277:1508–1510.
22. Welboren WJ, et al. (2009) ChIP-Seq of ERalpha and RNA polymerase II defines genes differentially responding to ligands. *EMBO J* 28:1418–1428.
23. Krishnakumar R, Kraus WL (2010) PARP-1 regulates chromatin structure and transcription through a KDM5B-dependent pathway. *Mol Cell* 39:736–749.
24. Petesch SJ, Lis JT (2008) Rapid, transcription-independent loss of nucleosomes over a large chromatin domain at Hsp70 loci. *Cell* 134:74–84.
25. Shang Y, Hu X, DiRenzo J, Lazar MA, Brown M (2000) Cofactor dynamics and sufficiency in estrogen receptor-regulated transcription. *Cell* 103:843–852.
26. Sheng S, Barnett DH, Katzenellenbogen BS (2008) Differential estradiol and selective estrogen receptor modulator (SERM) regulation of Keratin 13 gene expression and its underlying mechanism in breast cancer cells. *Mol Cell Endocrinol* 296:1–9.
27. Sun J, Nawaz Z, Slingerland JM (2007) Long-range activation of GREB1 by estrogen receptor via three distal consensus estrogen-responsive elements in breast cancer cells. *Mol Endocrinol* 21:2651–2662.
28. Fritah A, Redeuilh G, Sabbah M (2006) Molecular cloning and characterization of the human WISP-2/CCN5 gene promoter reveal its upregulation by oestrogens. *J Endocrinol* 191:613–624.
29. Han W, Pentecost BT, Pietropaolo RL, Fasco MJ, Spivack SD (2005) Estrogen receptor alpha increases basal and cigarette smoke extract-induced expression of CYP1A1 and CYP1B1, but not GSTP1, in normal human bronchial epithelial cells. *Mol Carcinog* 44: 202–211.
30. Tsuchiya Y, et al. (2004) Human CYP1B1 is regulated by estradiol via estrogen receptor. *Cancer Res* 64:3119–3125.
31. Cherrington BD, Morency E, Struble AM, Coonrod SA, Wakshlag JJ (2010) Potential role for peptidylarginine deiminase 2 (PAD2) in citrullination of canine mammary epithelial cell histones. *PLoS ONE* 5:e11768.
32. Voss TC, et al. (2011) Dynamic exchange at regulatory elements during chromatin remodeling underlies assisted loading mechanism. *Cell* 146:544–554.
33. Vic P, Garcia M, Humeau C, Rochefort H (1980) Early effect of estrogen on chromatin ultrastructure in endometrial nuclei. *Mol Cell Endocrinol* 19:79–92.
34. Luo Y, et al. (2006) Inhibitors and inactivators of protein arginine deiminase 4: Functional and structural characterization. *Biochemistry* 45:11727–11736.
35. Saldanha AJ (2004) Java Treeview—extensible visualization of microarray data. *Bioinformatics* 20:3246–3248.

Supporting Information

Zhang et al. 10.1073/pnas.1203280109

SI Materials and Methods

Cell Culture and E2 Treatments. MCF-7 cells were maintained in DMEM supplemented with 10% calf serum. The PAD2-depleted MCF-7 cell line was generated by transfection of MCF-7 cells with a Mission shRNA Plasmid DNA containing a short hairpin RNA (shRNA) construct targeting the human PAD2 coding sequence (Sigma; SHCLND-NM_007365) using FuGENE6 (Roche). The stable PAD4-depleted MCF-7 cell line was described (1). In the control group, cells were transfected with a nontargeting shRNA control vector (Sigma SHC002). Cells were selected by medium containing 1 μg/mL puromycin (Sigma). Flag-tagged PAD2 overexpression MCF-7 cells were generated by transfection with Flag-PAD2-pcDNA3.1 (+) and selected by medium containing 0.5 μg/mL puromycin. HeLa-ER cells were kindly provided by W. Lee Kraus (University of Texas Southwestern Medical Center, Dallas, TX). HeLa, HeLa-ER, and MDA-MB231 cells were maintained in DMEM supplemented with 10% (vol/vol) FBS. Before E2 treatment, the cells were cultured for 3 d in DMEM phenol red-free medium supplemented with 10% (vol/vol) charcoal-dextran–treated calf serum. ICI182780 was used at 10 μM for 18 h before the addition of E2.

Mouse Ovariectomy (OVX), E2 Treatment, and Immunohistochemistry (IHC). Female nu/nu nude mice (4-wk-old; The Jackson Laboratory) were ovariectomized and simultaneously implanted with s.c. estrogen pellets (0.72 mg per pellet, 60-d release; Innovative Research of America) or a sham control pellet ($n = 3$ per group). The mice were killed 3 wk after treatment. Uterine tissue was excised, fixed in 10% buffered formalin, embedded in paraffin, sectioned, and stained with anti-H3Cit26 antibody (Abcam; ab19847, lot 135757).

Confocal Microscopy. Cells grown on slides were subjected to E2 treatment for 45 min. Confocal microscopy experiments were described (2). Antibody used were as follows: anti-H3Cit26 (Abcam; ab19847, lot 135757), anti-H3Cit2/8/17 (Abcam; ab77164), H4Cit3 (Millipore; 07–596), Ac-H4K5 (Abcam; ab51997), H3K9 dimethyl (Abcam; ab1220), H3K27 trimethyl (Abcam; ab6002), and ERα (Abcam; ab2746). Images were collected with LSM 510 laser scanning confocal microscope (Carl Zeiss).

Chromatin Immunoprecipitation (ChIP) and ChIP-chip. ChIP experiments were performed as described (1). Estrogen was used at concentration of 100 nM for 45 min, Antibodies used were anti-H3Cit26 (Abcam; ab19847, lot 135757), anti-ERα (Santa Cruz; sc-542), and anti-Flag (Sigma; F3165). Primers used for the ChIP-qPCR were listed as below. ChIP for H3Cit26 coupled with hybridization to a human HG18 RefSeq promoter microarray from Nimblegen, and genomic data analyses were performed as described (1). The $\log_2$ ratio (IP/Input) data from each array was subjected to Lowess normalization (3). The normalized data were scaled to equivalent sum of squares and then the between-array mean $\log_2$ ratio was determined for each probe. An error model was generated by using a 1-kb moving window with 250-bp steps in which both the mean probe $\log_2$ ratio and P values were calculated for each window. The P values were calculated by using the nonparametric Wilcoxon signed-rank test. Significant peaks were defined as the center of three consecutive windows with positive means, the center window with a mean greater than either adjacent window, and all windows having significant P value less than 0.016. Induced regions were defined as H3Cit26-bound regions (present in the E2-treated samples) that had both a significant P value and a fold ratio >1.148 compared with the EtOH samples. Reduced regions were defined as H3Cit26-bound regions (present in the EtOH control samples) that had both a significant P value and a fold <1 compared with the E2-treated samples. Constitutive regions were defined as H3Cit26-bound regions (present in both conditions) that did not have a significant P value form the composite fold analysis. The TSS-anchored ChIP-chip heat maps were generated by using 600-bp windows with 150-bp steps and were visualized with Java Treeview (4). The data can be accessed through the NCBI/GEO website by using accession number GSE32599.

Steady-State Kinetic Assays. PAD2 was purified by established methods (5, 6). PAD4 was purified as described (7). Histone-based peptides were synthesized by using the Fmoc approach and purified by reverse-phase HPLC to ≥95%. Kinetic assays were performed as described (8). Briefly, reaction buffer (100 mM Tris·HCl at pH 7.6, 2 mM DTT, 10 mM CaCl2, and 50 mM NaCl) was preincubated for 10 min at 37 °C with varying concentrations of histone H3 (0–180 μM), or peptide (22–30) (0–10 mM). The reaction was initiated by the addition of enzyme (0.2 μM final). After 6 min, reactions were quenched by flash freezing in liquid nitrogen, and 200 μL of COLDER solution was added to each tube. The absorbance at 540 nm was quantified and product formation determined by comparing the absorbance to a citrulline standard curve. The data were fit to the following equation: $v = V_{max}[S]/(K_m+[S])$ by using the GraFit version 5.0.11 software package (9).

Acid Extraction of Histones, PAD Assay, and Western Blotting. MCF-7 cells were first E2 starved, followed by 100 nM E2 treatment for 45 min. EtOH treatment was used as a control. Cellular histones were purified by acid extraction (2). For the PAD assay, human PAD2 proteins were expressed and purified from pET16-PAD2 by using Ni-NTA Protein Purification System (Qiagen). The PAD assay was performed as described (2). Histone samples were separated by 15% SDS/PAGE, and the membrane was detected by Western blot using anti-H3Cit26 (ab19847, lot 135757), and anti-H3 (Abcam; ab1791).

Identification of Arg26 Citrullination in Human Histone H3 by nanoLC/MS/MS Analysis Using LTQ Orbitrap Velos. The PAD2-treated H3 bands were excised from gel and subjected to digestion and extraction as reported (10). The digest was reconstituted in 10 μL of 2% acetonitrile (ACN) with 0.5% formic acid (FA) for nanoLC-ESI-MS/MS analysis, which is carried out by using a LTQ-Orbitrap Velos (Thermo-Fisher Scientific) mass spectrometer equipped with "Plug and Play" nano ion source device (CorSolutions). The nanoLC was carried out by Dionex UltiMate3000 MDLC system (Dionex). The tryptic peptides (5–10 μL) was injected onto a PepMap C18 trap column at 20 μL/min flow rate and then separated on a PepMap C18 RP nano column, which was installed in the Plug and Play device with a 10-μm spray emitter (New Objective) mounted in front of Orbitrap orifice. The peptides were then eluted in a 90-min gradient of 10–40% ACN in 0.1% FA at 300 nL/min, followed by a 3-min ramping to 95% ACN-0.1% FA and a 5-min holding at 95% ACN-0.1% FA. The column was reequilibrated with 2% ACN-0.1% FA for 20 min before the next run. The Orbitrap Velos was operated in positive ion mode with nanospray voltage set at 1.5 kV and source temperature at 275 °C. Either internal calibration using the background polysiloxane ion signal at m/z 445.120025

as a lock mass or external calibration using Ultramark 1621 for Fourier Transform (FT) mass analyzer was performed. The instrument was performed in parallel data-dependent acquisition (DDA) mode by using FT mass analyzer for one survey MS scan for precursor ions followed by MS/MS scans on the top seven most intensity peaks with multiple charged ions above a threshold ion count of 7,500 in both LTQ mass analyzer and HCD-based FT mass analyzer at 7,500 resolution. MS survey scans at a resolution of 60,000 (FWHM at m/z 400), for the mass range of m/z 375–1800. Dynamic exclusion parameters were set at repeat count 1 with a 20-s repeat duration, exclusion list size of 500, 30-s exclusion duration, and ±10 ppm exclusion mass width. Collision induced dissociation (CID) parameters were set at the following values: isolation width 2.0 m/z, normalized collision energy 35%, activation Q at 0.25, and activation time 10 ms. The activation time is 0.1 ms for HCD analysis. All data are acquired under Xcalibur 2.1 operation software (Thermo-Fisher Scientific). All MS and MS/MS raw spectra were processed and searched by using Proteome Discoverer 1.2 (Thermo-Fisher Scientific) against Human RefSeq database downloaded from NCBInr database. The database search was performed with three-missed cleavage site by trypsin allowed. The peptide tolerance was set to 10 ppm, and MS/MS tolerance was set to 0.8 Da for CID and 0.05 Da for HCD. A fixed carbamidomethyl modification of cysteine, variable modifications on methionine oxidation, asparagine/glutamine deamidation, lysine acetylation/methylation, and arginine citrullination were set. The peptides with low confident score (with Xcorr score <2 for doubly charged ion and <2.7 for triply charged ion) defined by PD1.2 were filtered out, and the remaining peptides were considered for the peptide identification with possible modification determinations. All MS/MS spectra for possibly modified peptides identified from initial database searching were manually inspected and validated by using both PD1.2 and Xcalibur 2.1 software.

Immunoprecipitation Assay. MCF-7 cells and MCF-7 cells stably overexpressing Flag-tagged PAD2 were estrogen starved for 3 d followed by 100 nM E2 stimulation for 45 min at 37 °C. The whole-cell lysates were immunoprecipitated with anti-ER or anti-Flag M2 affinity gel (Sigma; A2220). Immunoprecipitates were analyzed by Western blot using anti-PAD2 (ProteinTech; 122100-1-AP), anti-ERα, and anti-Flag antibodies as indicated. The overexpression of Flag-PAD2 was verified by Western blot with anti-Flag and anti–β-actin (Sigma; A2066) antibodies.

Primers for ChIP-qPCR, RT-qPCR, and MNase Protection-qPCR.

ChIP-qPCR:
- TFF1 TSS1670-Fwd 5′-CCCACCTTTTCTCCAAATGA-3′
- TFF1 TSS1670-Rev 5′-GGTGGTTTTCGCTGCTCTAA-3′
- TFF1 TSS1339-Fwd 5′-AGAGGGGCTGCAGAAATGTA-3′
- TFF1 TSS1339-Rev 5′-GCTGCATGAAGAAATGGACA-3′
- TFF1 TSS1167-Fwd 5′-GCCACTGTTCTAGGGTCTGG-3′
- TFF1 TSS1167-Rev 5′-TGGGAGCAGAAGTCCTCATC-3′
- TFF1 TSS959-Fwd 5′-GAGCAGGAGGCTGTCCTCTA-3′
- TFF1 TSS959-Rev 5′-GTGGTTCACTCCCCTGTGTC-3′
- TFF1 TSS357-Fwd 5′-TTCCGGCCATCTCTCACTAT-3′
- TFF1 TSS357-Rev 5′-ATGGGAGTCTCCTCCAACCT-3′
- TFF1 TSS273-Fwd 5′-CCTGGATTAAGGTCAGGTTGGA-3′
- TFF1 TSS273-Rev 5′- TCTTGGCTGAGGGATCTGAGA-3′
- TFF1 TSS205-Fwd 5′- AGCCAAGATGACCTCACCAC-3′
- TFF1 TSS205-Rev 5′- TGGTCAAGCTACATGGAAGG-3′
- TFF1 TSS160-Fwd 5′- TTGTGGTTTTCCTGGTGTCA-3′
- TFF1 TSS160-Rev 5′- ACAGCAGCCCTTATTTGCAC-3′
- KRT13 TSS 1041-Fwd 5′-GTTACACCAGGGGTGTGGAG-3′
- KRT13 TSS 1041-Rev 5′-TTCCCAGCATTCCATAAAGG-3′
- KRT13 TSS 662-Fwd 5′-ACAGGGCCACTTCCTCTTTC-3′
- KRT13 TSS 662-Rev 5′-TTAGGGACCATCAGACACAGC-3′
- KRT13 TSS 620-Fwd 5′-TGTCTGATGGTCCCTAAGATCC-3′
- KRT13 TSS 620-Rev 5′-CGAGGCCATCAGAAAAAGTC-3′
- SCN1A TSS1083-Fwd 5′-CAAATAAAATTCATGGCCAAGTG-3′
- SCN1A TSS1083-Rev 5′-GCCAAAATATTCCAGAGCCTAA-3′
- SCN1A TSS823-Fwd 5′-TTGAGTTTATGGCACCCTGAC-3′
- SCN1A TSS823-Rev 5′-GTGCAGGAGACAGCAGGAGT-3′

RT-qPCR:
- TFF1-Fwd 5′-CATCGACGTCCCTCCAGAAGAG-3′
- TFF1-Rev 5′-CTCTGGGACTAATCACCGTGCTG-3′
- KRT13-Fwd 5′-GGCAGAGATGAGGGAGCAGTA-3′
- KRT13-Rev 5′-TCTTGGCGTGGAACCATTC-3′
- GREB1-Fwd 5′-CAAAGAATAACCTGTTGGCCCTGC-3′
- GREB1-Rev 5′-GACATGCCTGCGCTCTCATACTTA-3′
- CYP1B1-Fwd 5′-AACGTACCGGCCACTATC-3′
- CYP1B1-Rev 5′-CACGACCTGATCCAATTC-3′
- WISP2-Fwd 5′-GAGAGGCACACCGAAGAC-3′
- WISP2-Rev 5′-GGCAGGTACATGGTGTCG-3′
- SCN1A-Fwd 5′-CCTACATCGCCTGTTGGAC-3′
- SCN1A-Rev 5′-CCATGGAAACGTGGAAAGAA-3′
- VAT1L-Fwd 5′-CAAGAGCTTCTTCAGCTTTGC-3′
- VAT1L-Rev 5′-TTGATGGGGTTCACCTTCTC-3′
- ACTB-Fwd 5′-CCAACCGCGAGAAGATGA-3′
- ACTB-Rev 5′-CCAGAGGCGTACAGGGATAG-3′
- GAPDH-Fwd 5′-AGCCACATCGCTCAGACAC-3′
- GAPDH-Rev 5′-GCCCAATACGACCAAATCC-3′

MNase protection-qPCR:
- TFF1a-Fwd 5′-GCTTAGGCCTAGACGGAATG-3′
- TFF1a-Rev 5′-TGACCTTGCAGGGGGAAG-3′
- TFF1b-Fwd 5′-TTCATGAGCTCCTTCCCTTC-3′
- TFF1b-Rev 5′-GTGACAACAGTGGCTCACG-3′
- TFF1c-Fwd 5′-CCCGTGAGCCACTGTTGT-3′
- TFF1c-Rev 5′-TAGTGAGAGATGGCCGGAAA-3′
- TFF1d-Fwd 5′-TTCCGGCCATCTCTCACTAT-3′
- TFF1d-Rev 5′-CCCGCCAGGGTAAATACTGT-3′
- TFF1e-Fwd 5′-CGGGAGGGCCTCTCAGATA-3′
- TFF1e-Rev 5′-ATGGGAGTCTCCTCCAACCT-3′
- TFF1f-Fwd 5′-AAGGTCAGGTTGGAGGAGAC-3′
- TFF1f-Rev 5′-TGAGGGATCTGAGATTCAGAAAG-3′
- TFF1g-Fwd 5′-TCAGATCCCTCAGCCAAGAT-3′
- TFF1g-Rev 5′-TGGAAGGATTTGCTGATAGACA-3′
- TFF1h-Fwd 5′-TCACCACATGTCGTCTCTGTC-3′
- TFF1h-Rev 5′-TGGTCAAGCTACATGGAAGG-3′
- TFF1i-Fwd 5′-GCTTGACCATGTCTAGGAAACA-3′
- TFF1i-Rev 5′-CGGGGATCCTCTGAGACA-3′
- TFF1j-Fwd 5′-CAGTGGAGATTATTGTCTCAGAGG-3′
- TFF1j-Rev 5′-CGTTAGATAACATTTGCCTAAGGA-3′
- TFF1k-Fwd 5′-GGCCTCCTTAGGCAAATGTT-3′
- TFF1k-Rev 5′-AGCCCCGGATTTTATAGGG-3′
- KRT13a-Fwd 5′-TCAGTCCTGATTCTGCCCTTA-3′
- KRT13a-Rev 5′-CCACAGGAGGAGGGTCCTA-3′
- KRT13b-Fwd 5′-CATGTGTAAATGGGGGCAAT-3′
- KRT13b-Rev 5′-AGGCAGGAACTGGGTGAAGT-3′
- KRT13c-Fwd 5′-CTTCACCCAGTTCCTGCCTA-3′
- KRT13c-Rev 5′-AGTGGCCCTGTCCATTATCA-3′
- KRT13d-Fwd 5′-ACAGGGCCACTTCCTCTTTC-3′
- KRT13d-Rev 5′-TTAGGGACCATCAGACACAGC-3′
- KRT13e-Fwd 5′-TGTCTGATGGTCCCTAAGATCC-3′
- KRT13e-Rev 5′-CGAGGCCATCAGAAAAAGTC-3′
- KRT13f-Fwd 5′-GGCCTCGGAGCTATTTCTTT-3′
- KRT13f-Rev 5′-CGATAGAATCACCTGCCTTGA-3′
- KRT13g-Fwd 5′-TCAAGGCAGGTGATTCTATCG-3′
- KRT13g-Rev 5′-GGGATGTCCTGGATCCTTCT-3′

KRT13h-Fwd 5′-GGCCCCTGGAGTAGATGAAG-3′
KRT13h-Rev 5′-CTGACTGGGATGTCCTGGAT-3′
KRT13i-Fwd 5′-ATCCAGGACATCCCAGTCAG-3′
KRT13i-Rev 5′-CAGAGTGGCTCTGTGCTTTG-3′
KRT13j-Fwd 5′-ACTCTGCACCCACCACTTTC-3′
KRT13j-Rev 5′-AGAACGGGACCTGAGATGC-3′
WISP2a-Fwd 5′- GGCACCTCCATCAGAAAGTG-3′
WISP2a-Rev 5′- TTCAGGAATACCAGGCAAGG-3′
WISP2b-Fwd 5′- GGTATTCCTGAACTTCCACCTG -3′
WISP2b-Rev 5′- GAGGCACAACACTGACCTGA-3′
WISP2c-Fwd 5′- TCCTCAGGTCAGTGTTGTGC -3′
WISP2c-Rev 5′- GATGGGGTCAAGCCAAATC-3′
WISP2d-Fwd 5′- CAAATGGATTTGGCTTGACC -3′
WISP2d-Rev 5′- GGCAGGCTGGACCTACTATG-3′
WISP2e-Fwd 5′- CAAGCGCTGGCACATAGT -3′
WISP2e-Rev 5′- ATAAGGGGCCTCCCTTGG-3′
WISP2f-Fwd 5′- CCCTTATTGCCAAGAGCAAAC -3′
WISP2f-Rev 5′- TGACCCAGAGCAAAACTTCC-3′
WISP2g-Fwd 5′- GGAAGTTTTGCTCTGGGTCA -3′
WISP2g-Rev 5′- GGTTTCTGGCAGGCAGATT-3′
WISP2h-Fwd 5′- AATCTGCCTGCCAGAAACC -3′
WISP2h-Rev 5′- GTGGCCCTGACTCTGGGTAG-3′
WISP2i-Fwd 5′- CCACGGAGCTTAGGAGACCT -3′
WISP2i-Rev 5′- CAGTAAACAACCCCTTTGCAG-3′
WISP2j-Fwd 5′- AGCTCTGCAAAGGGGTTGTT -3′
WISP2j-Rev 5′- CCTATTCCAGACCCCCTGTC-3′
WISP2k-Fwd 5′- GACAGGGGGTCTGGAATAGG -3′
WISP2k-Rev 5′- AGGGTCCTAGCCCTGCTGTA-3′
GREB1a-Fwd 5′- GGAAACAGATGGGAAAGACAA-3′
GREB1a-Rev 5′- CCTCGCTCCAAGACCAGA-3′
GREB1b-Fwd 5′- CCTAGGAGCTCTGGTCTTGG -3′
GREB1b-Rev 5′- TGGCCACAATTGAACATAGG-3′
GREB1c-Fwd 5′- TGTTCAATTGTGGCCAATAAA -3′
GREB1c-Rev 5′- CAAGCCCTGATCAAGGAAAC-3′
GREB1d-Fwd 5′- GTTTCCTTGATCAGGGCTTG -3′
GREB1d-Rev 5′- TTTGCTCAAAGTGAGGACGTT-3′
GREB1e-Fwd 5′- TCCTCACTTTGAGCAAAAGC -3′
GREB1e-Rev 5′- AACAAAAACTAAAGGCGTAAGGA-3′
GREB1f-Fwd 5′- CGCCTTTAGTTTTTGTTTAAAGGT -3′
GREB1f-Rev 5′- ATGACCCAGTTGCCACACTT-3′
GREB1g-Fwd 5′- AGTGTGGCAACTGGGTCATT -3′
GREB1g-Rev 5′- GCTGCGGCAATCAGAAGTAT-3′
GREB1h-Fwd 5′- CCGCAGCAGACAATGATG -3′
GREB1h-Rev 5′- TGAAAAGGCAGCAAACTTGT-3′
GREB1i-Fwd 5′- CTTTTCATTTCTGTGGGTCGT -3′
GREB1i-Rev 5′- ACAGACCCAAACATGCTGCT-3′
GREB1j-Fwd 5′- AGCAGCATGTTTGGGTCTGT -3′
GREB1j-Rev 5′- CTAGTGGGGACAAGCACACA-3′
GREB1k-Fwd 5′- GTGTGTGCTTGTCCCCACTA -3′
GREB1k-Rev 5′- TGGACAAGCCATATCCCTAA-3′
CYP1B1a-Fwd 5′- GCCGCAAGAACTGGAAAA -3′
CYP1B1a-Rev 5′- ACCTCAGTGGAGGCTCTTTG-3′
CYP1B1b-Fwd 5′- CTCCACTGAGGTGGCAATTT -3′
CYP1B1b-Rev 5′- GCCCCTGGTTGGTTGTTTA-3′
CYP1B1c-Fwd 5′- GCTGCCACTACACTGGCTTT -3′
CYP1B1c-Rev 5′- ACGACCTCCCTTCCCTCTC-3′
CYP1B1d-Fwd 5′- GGAGAGGGAAGGGAGGTC -3′
CYP1B1d-Rev 5′- CCACGCTCGGTACAACCT-3′
CYP1B1e-Fwd 5′- GTTGTACCGAGCGTGGTTCT -3′
CYP1B1e-Rev 5′- ACGTTTCCATTGTGCGGTA-3′
CYP1B1f-Fwd 5′- GTTACCGCACAATGGAAACG -3′
CYP1B1f-Rev 5′- GCTCTACCAGCAGGCTTTCA-3′
CYP1B1g-Fwd 5′- ACCTCCGCTCCCATGAAA -3′
CYP1B1g-Rev 5′- ACACCAGGCCGCTTTGAC-3′
CYP1B1h-Fwd 5′- GTCAAAGCGGCCTGGTGT -3′
CYP1B1h-Rev 5′- TCCTCCGGGTTTTAAGGACT-3′
CYP1B1i-Fwd 5′- CCTCCTTCTACCCAGTCCTTAAA -3′
CYP1B1i-Rev 5′- TCCCACTCCCACTCCAGA-3′
CYP1B1j-Fwd 5′- TGACTCTGGAGTGGGAGTGG -3′
CYP1B1j-Rev 5′- CTCACAACTGGAGTCGCAGA-3′
SCN1Aa-Fwd 5′-CAAATAAAATTCATGGCCAAGTG-3′
SCN1Aa-Rev 5′-GCCAAAATATTCCAGAGCCTAA-3′
SCN1Ab-Fwd 5′-TCTGGAATATTTTGGCTCAGTAAT-3′
SCN1Ab-Rev 5′-GACGCCAAATCCCAAATGTA-3′
SCN1Ac-Fwd 5′-ACATTTGGGATTTGGCGTCT-3′
SCN1Ac-Rev 5′-AAAACCGTCAACCCCATACA-3′
SCN1Ad-Fwd 5′-TGTATGGGGTTGACGGTTTT-3′
SCN1Ad-Rev 5′-TGAAATTCTTGCTGATTCTATAGTCC-3′
SCN1Ae-Fwd 5′-CAAGAATTTCATTATTGCTTCAGTG-3′
SCN1Ae-Rev 5′-TCAGGGTGCCATAAACTCAA-3′
SCN1Af-Fwd 5′-TTGAGTTTATGGCACCCTGAC-3′
SCN1Af-Rev 5′-GTGCAGGAGACAGCAGGAGT-3′
SCN1Ag-Fwd 5′-GAGACTCCTGCTGTCTCCTG-3′
SCN1Ag-Rev 5′-GGTGGGGGTGGAAGAAGATA-3′
SCN1Ah-Fwd 5′-ATCTTCTTCCACCCCCACCT-3′
SCN1Ah-Rev 5′-GAAGGAGAGGAAAACTAGGCTGT-3′
SCN1Ai-Fwd 5′-CAGCCTAGTTTTCCTCTCCTTC-3′
SCN1Ai-Rev 5′-AGTCCACGGTTGGACAAATG-3′
SCN1Aj-Fwd 5′-GTCCAACCGTGGACTGTCTT-3′
SCN1Aj-Rev 5′-TGTCCTGCTCACTTCACTAGC-3′
VAT1La-Fwd 5′-GGGCATTTAAAGCAGTGAGG-3′
VAT1La-Rev 5′-AAGTGCTGCCTCTTCTCTCC-3′
VAT1Lb-Fwd 5′-GGGAGAGAAGAGGCAGCACT-3′
VAT1Lb-Rev 5′-TCAGAGCATGAGGCATGAAG-3′
VAT1Lc-Fwd 5′-ACTGTGTCCTTCATGCCTCA-3′
VAT1Lc-Rev 5′-TGGGGTGGACATGATTTCAG-3′
VAT1Ld-Fwd 5′-TGTCTCACTGAAATCATGTCCA-3′
VAT1Ld-Rev 5′-TTTTTCTATATTGTGTGAAGTGCTG-3′
VAT1Le-Fwd 5′-ACCCCAGCACTTCACACAAT-3′
VAT1Le-Rev 5′-CCTGAGCCTCAACACACTCA-3′
VAT1Lf-Fwd 5′-TGTTGAGGCTCAGGAAGGTT-3′
VAT1Lf-Rev 5′-TGCAGGTGAGGAAGTAGGTCT-3′
VAT1Lg-Fwd 5′-CCTCACCTGCATCTCTTTCC-3′
VAT1Lg-Rev 5′-GGAAGGACGTGGTTTTCCTA-3′
VAT1Lh-Fwd 5′-ACTGCCCCTAGGAAAACCAC-3′
VAT1Lh-Rev 5′-GGCTCTTTGAGAAAAACAGCTC-3′
VAT1Li-Fwd 5′-CTGTTTTTCTCAAAGAGCCTGA-3′
VAT1Li-Rev 5′-TGCATGCACATACACAGAGTAG-3′
VAT1Lj-Fwd 5′-TGTATGTGCATGCATGTTGG-3′
VAT1Lj-Rev 5′-GTGTTCTGATCCCCGGAAG-3′
VAT1Lk-Fwd 5′-GAGCGGGTACACACTGGTCT-3′
VAT1Lk-Rev 5′-CACCATTTCGGGCTATTAAAGA-3′

1. Zhang X, et al. (2011) Genome-wide analysis reveals PADI4 cooperates with Elk-1 to activate c-Fos expression in breast cancer cells. *PLoS Genet* 7:e1002112.
2. Wang Y, et al. (2004) Human PAD4 regulates histone arginine methylation levels via demethylimination. *Science* 306:279–283.
3. Smyth GK, Speed T (2003) Normalization of cDNA microarray data. *Methods* 31: 265–273.
4. Saldanha AJ (2004) Java Treeview—extensible visualization of microarray data. *Bioinformatics* 20:3246–3248.
5. Knuckley B, et al. (2010) Substrate specificity and kinetic studies of PADs 1, 3, and 4 identify potent and selective inhibitors of protein arginine deiminase 3. *Biochemistry* 49:4852–4863.
6. Raijmakers R, et al. (2007) Methylation of arginine residues interferes with citrullination by peptidylarginine deiminases in vitro. *J Mol Biol* 367:1118–1129.
7. Knuckley B, Bhatia M, Thompson PR (2007) Protein arginine deiminase 4: Evidence for a reverse protonation mechanism. *Biochemistry* 46:6578–6587.
8. Kearney PL, et al. (2005) Kinetic characterization of protein arginine deiminase 4: a transcriptional corepressor implicated in the onset and progression of rheumatoid arthritis. *Biochemistry* 44:10570–10582.
9. Leatherbarrow RJ (2004) *Grafit Ver 5.0* (Erathicus Software, Staines, UK).
10. Zhang S, Van Pelt CK, Henion JD (2003) Automated chip-based nanoelectrospray-mass spectrometry for rapid identification of proteins separated by two-dimensional gel electrophoresis. *Electrophoresis* 24:3620–3632.

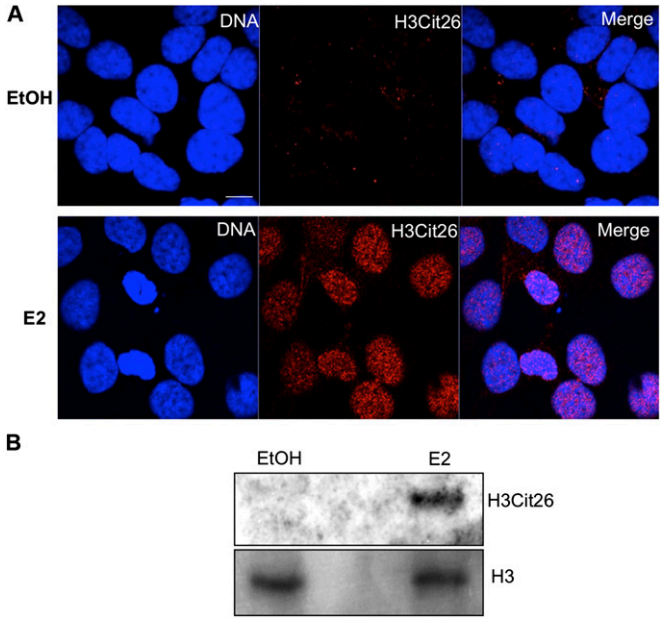

Fig. S1. E2 induced global activation of H3R26 citrullination in MCF-7 cells. (*A*) In the absence of E2 treatment (EtOH control), H3Cit26 signals (red) are very weak. After 45 min of E2 treatment, elevated levels of nuclear H3R26 citrullination are observed. (Scale bar: 10 μm.) (*B*) Western blot showing that amounts of H3Cit26 were increased in MCF-7 cells after E2 treatment. Blotting with anti-Histone H3 (*Lower*) revealed that histone levels between groups were similar.

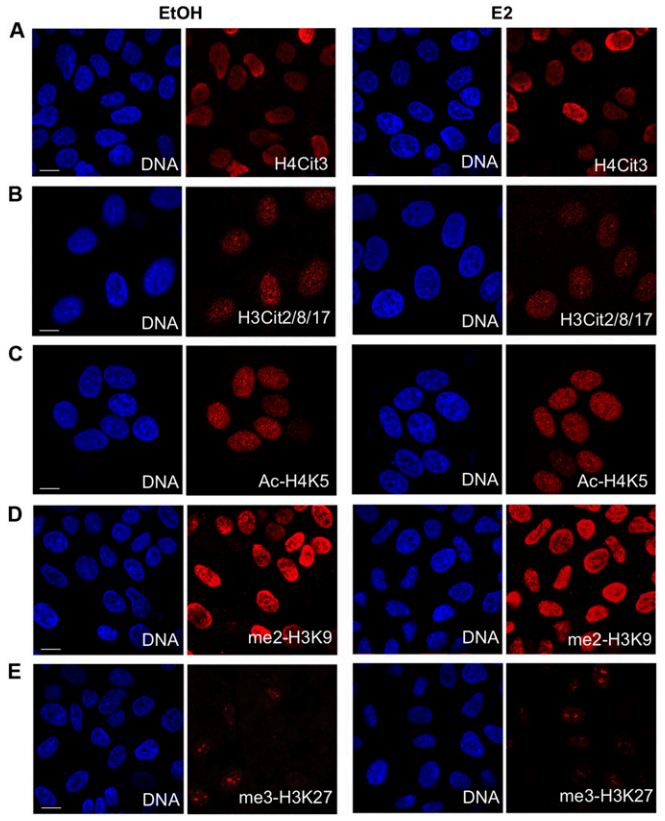

Fig. S2. Estrogen treatment does not appear to globally affect levels of other histone modifications in MCF-7 cells. Confocal immunofluorescence images show that the signals for H4Cit3 (*A*), H3Cit2/8/17 (*B*), Ac-H4K5 (*C*), me2-H3K9 (*D*), and me3-H3K27 (*E*) signals do not appear to change after E2 stimulation. (Scale bars: 10 μm.)

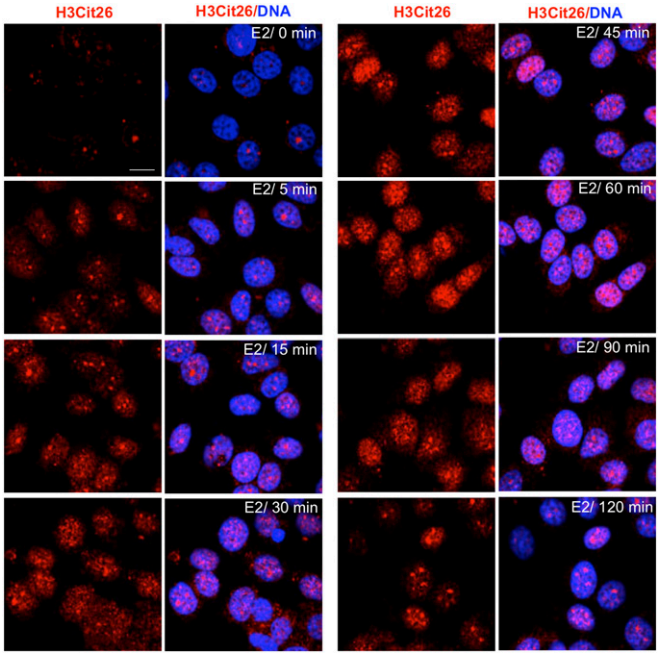

Fig. S3. Time course of E2-induced global H3R26 citrullination in MCF-7 cells. Confocal immunofluorescence microscopic images showing that treatment of estrogen-starved MCF-7 cells with 100 nM of E2 results in H3R26 citrullination within 5 min and that the signal peaked at 45 min after E2 treatment. (Scale bar: 10 μm.)

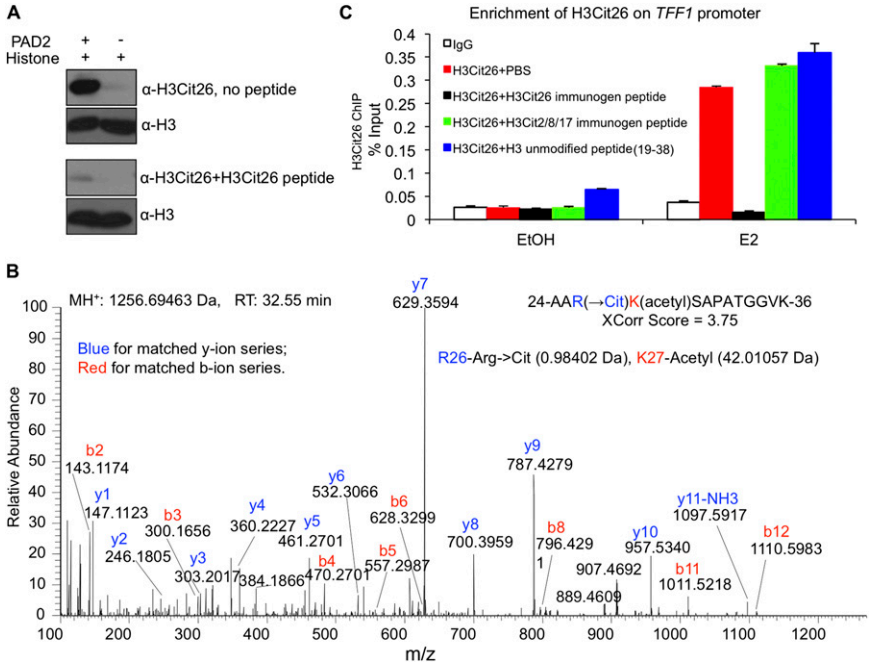

Fig. S4. H3Cit26 antibody specificity. (*A*) Specificity of the anti-H3Cit26 antibody was tested with peptide competition assay. Western blot showing that the anti-H3Cit26 antibody is specifically reactive with the appropriately sized band from human PAD2-treated MCF-7 cell histones but not from nontreated histones. Anti-H3Cit26 antibody was preincubated with 1 μg/mL H3Cit26 immunogen peptide (Abcam; ab20631) overnight at 4 °C before Western blot analysis. The competing peptide nearly completely blocked detection of H3Cit26. Anti-histone H3 staining revealed the presence of approximately equal amounts of histone in each lane. (*B*) The positive band in *A* was subjected to MS/MS analysis. Citrullination at R26 of the tryptic peptide AARKSAPATGGVK from human histone 3 was detected by nanoLC-MS/MS analysis. MS/MS spectrum of the doubly charged peptide ions at *m/z* $[628.8510]^{2+}$ with elution time at 32.55 min shows almost all y-ion series and b-ion series, demonstrating that R26 residue was converted to Citrulline (Arg > Cit) with increased 0.98402 Da. Meanwhile, K27 was identified as being acetylated (42.01057 Da). The MS/MS spectrum was searched against human database by using Proteome Discoverer 1.2 software with integrated SEQUEST searching engine with XCorr:3.75, and Probability:51.10. (*C*) ChIP analysis showing that H3Cit26 enrichment on TFF1 promoter is specifically competed by the H3Cit26 immunogen peptide. Anti-H3Cit26 antibody was mock- (PBS incubation) or preincubated with 1 μg/mL H3Cit26 immunogen peptide (Abcam; ab20631), H3Cit2/8/17 immunogen peptide (Abcam; ab32876), or unmodified histone H3 (19–38) overnight at 4 °C. IgG was used as a control.

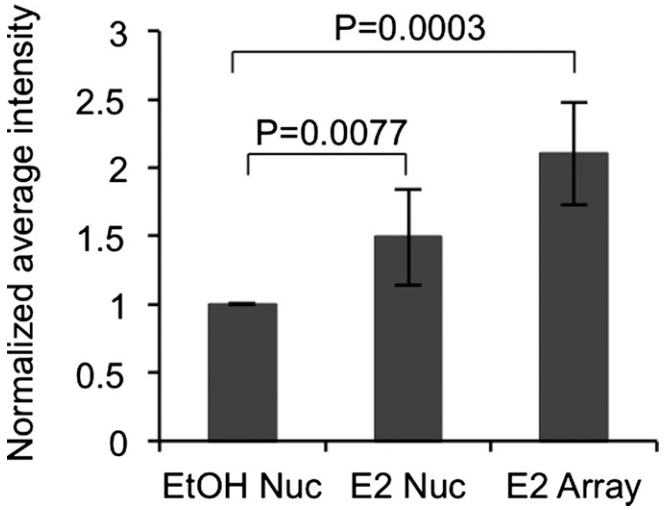

Fig. S5. Quantitation of H3Cit26 at the PRL-array. The histogram shows relative intensity for the anti-H3Cit26 signal in E2-treated nucleoplasm (E2 Nuc) and E2-treated array (E2 Array) compared with EtOH treated nucleoplasm (EtOH Nuc). *P* values were calculated based on the basis of two-tailed Student *t* test.

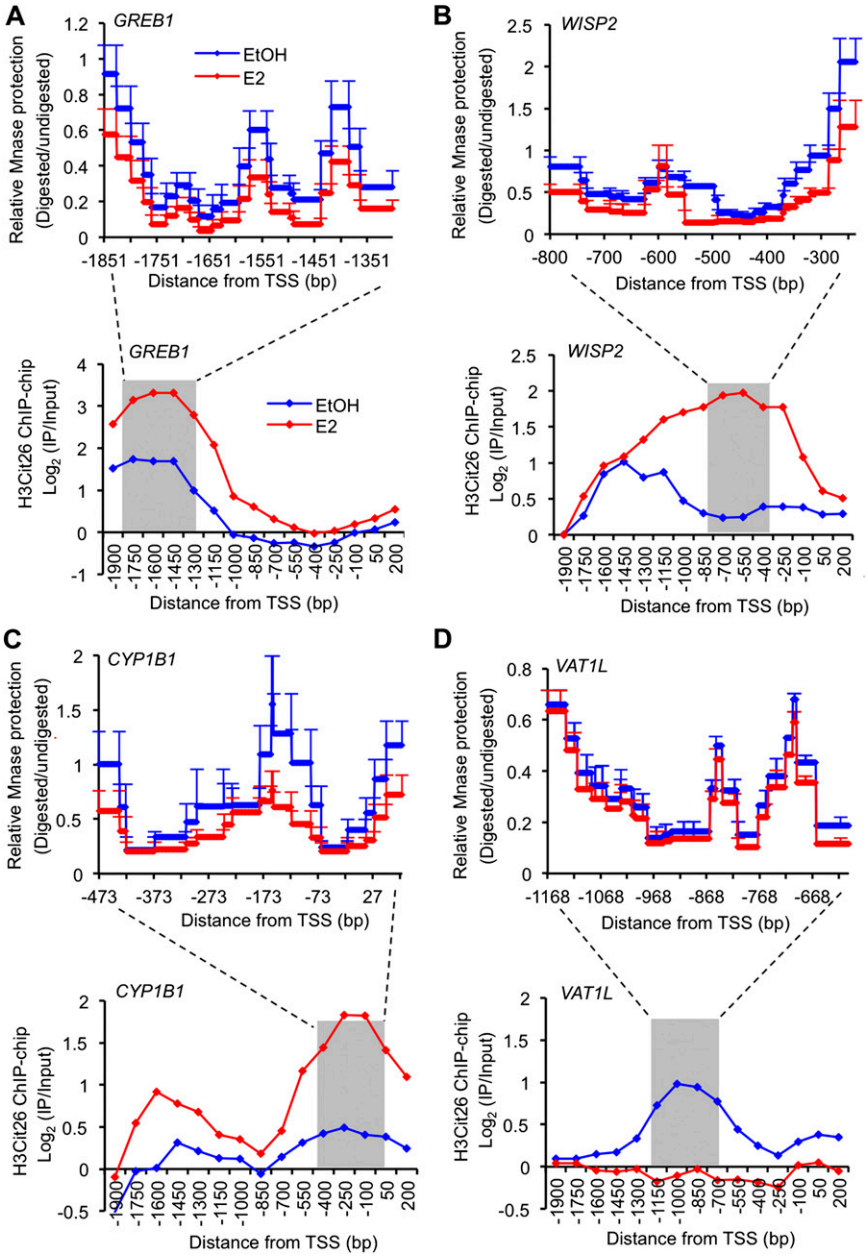

Fig. S6. After estrogen stimulation, H3R26 citrullinaton facilitates an open chromatin architecture at the EREs of E2-induced gene promoters. In each graph, GREB1 (*A*), WISP2 (*B*), CYP1B1 (*C*), or VAT1L (*D*), *Upper* shows the MNase protection assay following EtOH or E2 treatment in MCF-7 cells. qPCR was performed to tile through the proximal promoter ERE region with overlapping amplicons (~100-bp PCR product average, with ~20-bp overlap). Relative ratio of the amount of digested DNA to genomic control was used to determine the extent of MNase protection. Values from overlapping primer sets are averaged. Each point represents the mean + SEM, $n = 3$. *Lower* shows the H3Cit26 ChIP-chip signal at the proximal promoter ERE region of E2-induced target.

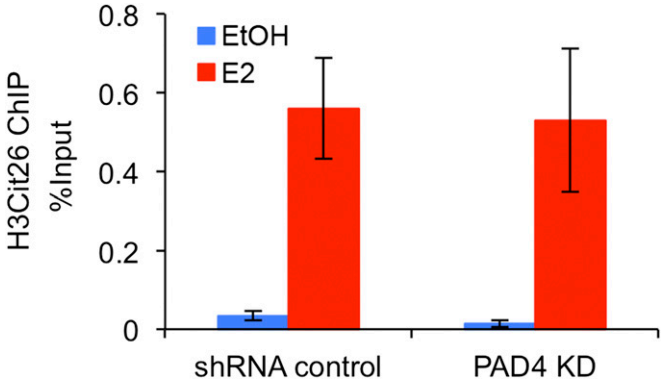

Fig. S7. Depletion of PAD4 does not inhibit H3Cit26 enrichment on *TFF1* ERE region. Depletion of PAD4 (PAD4 KD) from MCF-7 cells was described (3). E2 treatment induced the pronounced enrichment of H3Cit26 on the *TFF1* ERE region in the shRNA control MCF-7 cells, whereas this increase was not observed in the PAD4 depleted line.

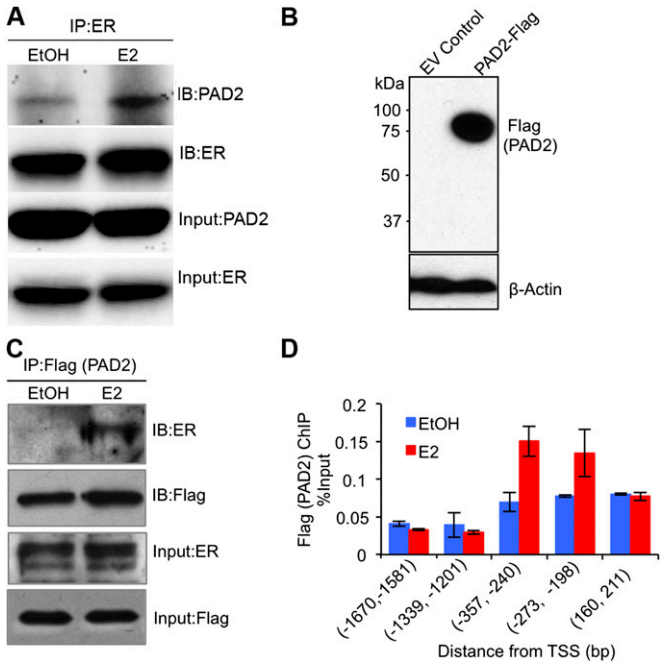

Fig. S8. E2 stimulates the association of PAD2 with ER at the ERE region on the *TFF1*. (*A*) Coimmunoprecipitation analysis in wild-type MCF-7 cells reveals that E2 treatment stimulates the interaction between endogenous PAD2 and ER. (*B*) Western blotting documenting PAD2 overexpression. EV represents the empty vector control. β-actin (*Lower*) revealed equal protein loading. (*C*) Coimmunoprecipitation analysis of MCF-7 cells stably overexpressing Flag-PAD2 reveals that E2 treatment stimulates the interaction between endogenous ER and ectopically expressed PAD2. (*D*) Ectogenic PAD2 is recruited to TFF1 ERE promoter region after E2 treatment. ChIP assay with anti-Flag antibody on the TFF1 tilling promoter regions in the MCF-7 cells stably overexpressing PAD2. E2 stimulation induced PAD2 recruitment to the ERE region.

Table S1. Steady-state kinetic parameters for histone H3 and H4 substrates

Enzyme	Substrate	k_{cat}, s^{-1}	K_m, mM	k_{cat}/K_m, $s^{-1}\cdot M^{-1}$
PAD2	H3	ND*	ND*	1,200
	H3 (1–15)	2.4 + 0.10	1.9 + 0.25	1,250
	H3 (22–30)	1.4 + 0.17	3.7 + 1.0	370
	H4	ND*	ND*	2,400
	H4 (1–15)	1.4 + 0.1	1.0 + 0.2	1,400
PAD4	H3	ND*	ND*	3,700[†]
	H3 (1–15)	0.6 + 0.03	3.3 + 0.4	180
	H3 (22–30)	ND*	ND*	60
	H4	1.2 + 0.2[‡]	0.1 + 0.03[‡]	9,000[‡]
	H4 (1–15)	2.5 + 0.1	0.6 + 0.1	4,400

Kinetic parameters were measured by incubating the enzyme at 37 °C.
*ND, not determined due to a lack of saturation in the *v* versus [S] curves.
[†]Value taken from ref. 1.
[‡]Value taken from ref. 2.

1. Slack JL, Causey CP, Luo Y, Thompson PR (2011) Development and use of clickable activity based protein profiling agents for protein arginine deiminase 4. *ACS Chem Biol* 6:466–476.
2. Knuckley B, et al. (2010) Substrate specificity and kinetic studies of PADs 1, 3, and 4 identify potent and selective inhibitors of protein arginine deiminase 3. *Biochemistry* 49:4852–4863.

Table S2. ERE matrix file found by MEME from the 208 E2-induced H3Cit26 binding sites

Position	"A"	"C"	"G "	"T"
1	0.048780	0.000000	0.658537	0.292683
2	0.000000	0.073171	0.926829	0.000000
3	0.000000	0.000000	0.000000	1.000000
4	0.000000	1.000000	0.000000	0.000000
5	1.000000	0.000000	0.000000	0.000000
6	0.073171	0.585366	0.341463	0.000000
7	0.414634	0.292683	0.121951	0.170732
8	0.000000	0.341463	0.487805	0.170732
9	0.146341	0.000000	0.000000	0.853659
10	0.073171	0.195122	0.682927	0.048780
11	0.243902	0.170732	0.292683	0.292683
12	0.170732	0.829268	0.000000	0.000000
13	0.000000	0.634146	0.000000	0.365854
14	0.097561	0.121951	0.097561	0.682927
15	0.024390	0.243902	0.243902	0.487805